Acta Oceanol. Sin., 2019, Vol. 38, No. 5, P. 129–133
https://doi.org/10.1007/s13131-019-1444-0
http://www.hyxb.org.cn
E-mail: hyxbe@263.net

Multibeam water column data research in the Taixinan Basin: Implications for the potential occurrence of natural gas hydrate

Yilan Chen[1], Jisheng Ding[1]*, Haiquan Zhang[1], Qiuhua Tang[1], Xinghua Zhou[1], Xiaoyu Liu[1]

[1] First Institute of Oceanography, Ministry of Natural Resources, Qingdao 266061, China

Received 1 February 2018; accepted 27 April 2018

Abstract

A multi beam sonar survey is carried out in the continental slope of the Taixinan Basin to obtain submarine topographic and water column data. The data are processed to obtain water column images. Anomalous water column images, displaying plume characteristics, are found in gas hydrate enriched areas in the Taixinan Basin. This indicates the presence of natural gas resources in the Taixinan Basin. The multibeam sonar system is shown to provide an accurate and effective approach for detecting sub-sea gas hydrate.

Key words: multibeam sonar, water column image, plume flow, Taixinan Basin, gas hydrate

Citation: Chen Yilan, Ding Jisheng, Zhang Haiquan, Tang Qiuhua, Zhou Xinghua, Liu Xiaoyu. 2019. Multibeam water column data research in the Taixinan Basin: Implications for the potential occurrence of natural gas hydrate. Acta Oceanologica Sinica, 38(5): 129–133, doi: 10.1007/s13131-019-1444-0

1 Introduction

In recent decades, the multibeam sonar system has been widely used in underwater topographic surveys because of its full coverage, high resolution, high precision, and high efficiency. The multibeam survey has become a main investigation method for the underwater topography surveys. In addition to the development of underwater multibeam sonar systems, and the development of computer processing and storage, a large amount of marine acoustic information has been collected. This information is not only used in hydrographic surveying, but also in the fields of marine biology, physical oceanography, marine geology, and geophysics. Many researchers have done studies based on multibeam sonar data. The sonar data can be used to detect fish schools, plankton, internal waves, and hydrothermal vents, and to identify ocean habitats (Yang et al., 2013; Colbo et al., 2014; Melvin and Cochrane, 2015; Bayrakci et al., 2014). In recent years, multibeam water column data have been used to detect natural gas vents. For example, Elhegazy (2011) used water column images to detect and analyze undersea black smokers and natural gas vents. Nakamura et al. (2015) detected many undersea hydrothermal vents in the central area of the Okinawa Trough using multibeam water column images. These examples show that multibeam water column image investigations are an effective method for detecting the hydrothermal vents. Multibeam sonar images can be used to rapidly detect areas where hydrothermal fluids and cold seepages have developed, and provide new approaches for the detection of undersea resources. Geophysical methods have often been used to detect oil and gas resources (Luan et al., 2008; Xu et al., 2012), but the efficiency of these methods was low. Because the multibeam systems can acquire and process data more quickly and efficiently, the application of the multibeam water column data to hydrocarbon exploration will greatly improve the efficiency of oil and gas exploration. In the multibeam sonar approach, possible target areas for oil and gas resources are quickly delineated. Then, the geological, geophysical and geochemical surveys of the target area are carried out. This approach can save on costs and improve the success rate of oil and gas detection. The present study the analyses water column data from the multibeam sonar for natural gas detection in the Taixinan Basin.

2 Brief introduction to the research area

The Taixinan Basin is also known as the Tainan Basin. It is located on the continental slope from the southern part of the Taiwan Strait to the northeastern South China Sea, and forms part of China's offshore basins. Its geographic range is 20°50′–23°30′N, 117°00′–120°40′E (Fig. 1). The basin is centered on 22°N and 119°E, and is orientated in a NE–SW orientation. The length of the basin is about 480 km, and the width is about 240 km (Du et al., 1991). The total area is 72 000 km^2. The Taixinan Basin belongs to the rift-type (opening mode), Meso-Cenozoic superimposed or residual basin. The basin has the Penghu-Kaohsiung uplift as its northern boundary, and connects to the South China Sea Basin in the south. The Tainan-Kaohsiung epicontinental area forms its eastern boundary and the basin connects to the Chaoshan sag and Zhujiang River Mouth Basin in the west. The Taixinan Basin is one of the Meso-Cenozoic superimposed basins in the northern epicontinental sedimentary basin chain of the South China Sea. It is located in a favorable tectonic area for natural-gas enrichment. The characteristics of hydrocarbon migration and accumulation in the Taixinan Basin are similar to those of the continental fault basins in eastern China (He et al., 2006). Many studies have shown that the Taixinan Basin has abundant conventional oil and gas resources, and a large exploration potential for gas hydrates. Du et al. (1994) identified the Taixinan Basin as being a favorable area for oil and gas explora-

Foundation item: The National Key R&D Program of China under contract No. 2017YFC0306003; the National Natural Science Foundation of China under contract Nos 41506069, 41876111 and 40706038.
*Corresponding author, E-mail: dingjisheng@fio.org.cn

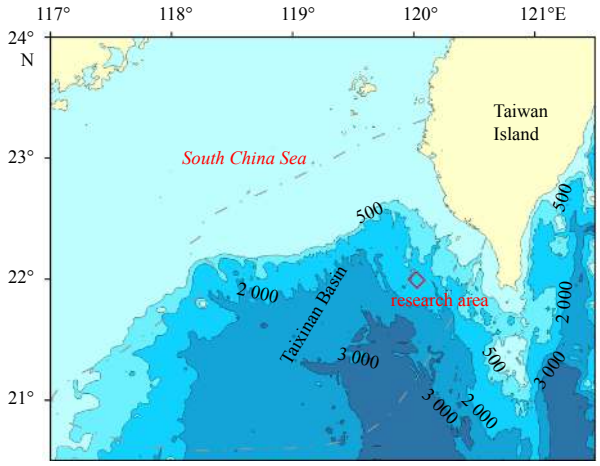

Fig. 1. Location of the research area (– – basin boundary from Ma (2016)).

tion. Oung et al. (2006) analyzed seafloor sediment samples collected southwest of Taiwan and detected thermogenic gas. Using a deeply-towed, side-scan sonar, subbottom profiler, Chen et al. (2010) discovered gas seepages in the nearshore area of the Taixinan Basin. Zhang et al. (2014) studied the accumulation characteristics of gas hydrates of the Taixinan Basin using samples from drillings. A bottom simulating reflector (BSR) obtained from geophysical surveys also showed the existence of gas hydrates in the area, and indicated that there were large accumulations of gas hydrates (Zhang et al., 2014). However, there are no studies that document using the multibeam sonar and the water column images to search for oil and gas on the eastern continental slope of the Taixinan Basin (Fig. 1). The present study helps address this knowledge gap.

3 Data and methods

3.1 *Data acquisition*

In 2016, we carried out sonar data acquisition in the Taixinan Basin using a Kongsberg EM302 deep-water, multibeam system. Three lines were used and were surveyed in both directions to give a total of six survey lines (Fig. 2). Repeat surveys were done to ensure data validity (Fig. 2). The performance parameters of

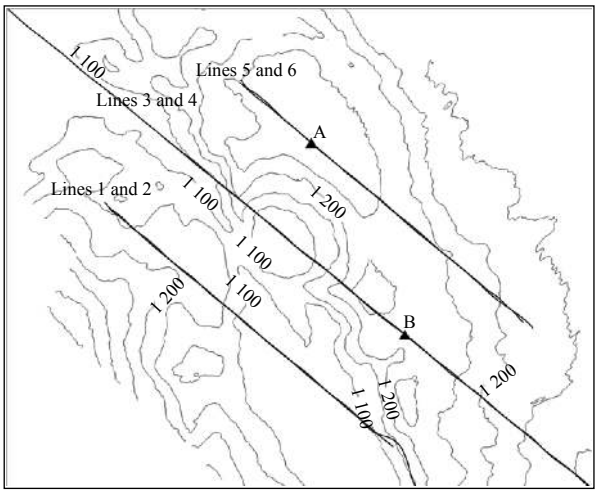

Fig. 2. Survey line setting.

the Kongsberg EM302 system are as follows: frequency 30 kHz, depth range 10–7 000 m, beam angle 1°×1°, maximum ping rate greater than 10 Hz, and beams in each ping 288. The multibeam system also acquires depth data and water column data, which are saved in the same data file to facilitate data processing.

3.2 *Data processing and display*

3.2.1 *Data processing*

Data processing included depth data processing and water column data processing. The depth data processing focused on signal filtering to remove erroneous data and display the authentic bottom topography. The filtering was performed by combining automatic filtering and manual filtering, and by setting the threshold values of, for example, beam and water depth. On the basis of the known water depth of the survey area the depth threshold was set at 800–1 600 m. Twenty edge beams were filtered out because edge beams are of poor quality. However, the automatic filtering cannot eliminate all outliers. The remaining outliers were manually removed. The water column data processing also focused on filtering to remove noise and retain the geographical features of the target. The water column data are time series observation values of the echo intensity for each beam footprint. The volume of water column data is ten to one hundred times that of the depth data (Liu, 2013). The echo intensity information is mainly used for the filtering of the sampling points of the water column data. The back scattering characteristics of acoustic signals for different materials are different. Normally, the echo intensity of noise and side lobe effects in water are low, and thus the echo intensity information can be used for the filtering of sampling points whose echo intensity signal is beyond the threshold. The echo intensity parameter was set between –60 and 0 dB.

3.2.2 *Displaying water column data*

The water column data can be displayed as a water column image to intuitively depict the water data and identify special targets in water. The water column data can be displayed in two ways: (1) as a cross-section perpendicular to the track direction, with the variation in a water intensity in each ping perpendicular to the track direction. The abscissa axis is a distance, and the ordinate axis is a water depth (Fig. 3); and (2) along the track section, with the variation in the central part of the water intensity along the track direction clearly visible (Liu, 2013; Zheng et al., 2016). The abscissa axis is time, and the ordinate axis is the water depth (Fig. 4). The colors of the images represent a back-scatter-

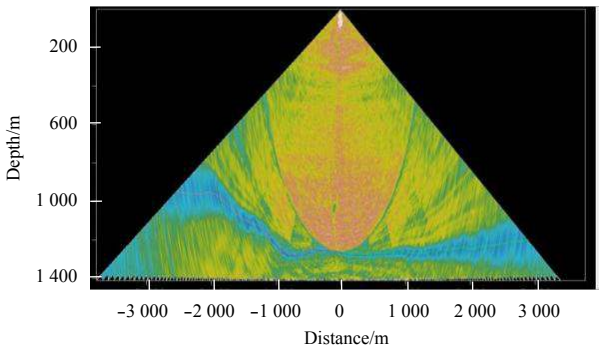

Fig. 3. Water image cross-section perpendicular to the track direction, where the abscissa axis is the distance to the center beam and the ordinate axis is the depth.

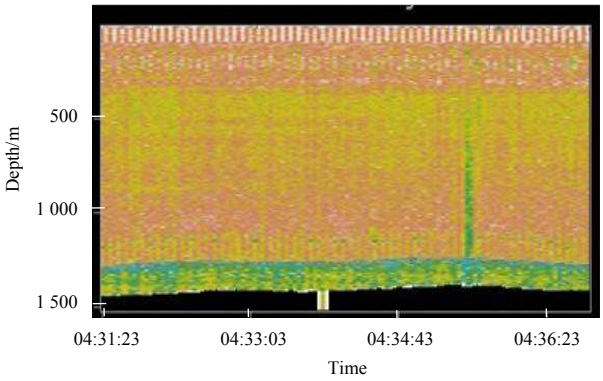

Fig. 4. Water image cross-section along the track direction, where the abscissa axis is time and the ordinate axis is the depth.

ing intensity.

4 Results and discussion

4.1 *Water image data results*

The multibeam water column images were obtained by processing and displaying the multibeam data. Lines 3 and 4 represent different measuring directions along the same line. Acoustic water column anomalies were found in the same region (Figs 5 and 6). Lines 5 and 6 are back and forth measurements along the same line. The acoustic water column anomalies were also found in the same region (Fig. 7). No obvious water column anomalies were found in Lines 1 and 2. The water columns in Fig. 7 are located at Position A in Fig. 2. The water columns in Figs 5 and 6 are located at Position B in Fig. 2. The image on the left of Fig. 5 shows the water column image at a specific time, while the image on the right shows a stacked view of all the water column images at Position B. The two images in Fig. 6 represent the water column images at different times at Position A.

No beams were lost on Line 3, but many beams were lost on Line 4, and thus the quality of Line 3 is much higher than that of Line 4, even though the section tracks are the same. Similarly, although a significant beam loss occurred because of difficult sea conditions during the survey of Lines 5 and 6, the water column anomalies were still captured. Figure 5 shows that the water column anomalies take the form of one or more acoustic scattering plumes that rise from the seafloor (the max height is about 500 m). Some ascending plumes are continuous, while some are not continuous. Most plumes are changeable. The ascending height of the water column anomalies shown in Fig. 6 is nearly identical to that in Fig. 5, but most plumes are suspended. The ascending height of the water column anomalies (Fig. 7) is about 200 m, and is not continuous. The width of the plumes is 20–50 m. The plumes are slightly curved. The lower parts all display vertical movement, and there is only a slight inclination in the upper area.

4.2 *Discussion*

4.2.1 *Causes of the scattering anomalies*

The water column images show that there are many plume-like anomalies in the study region. A seafloor plume is a typical expression of gas seepage. A large volume of gas is generated, probably from the lower part of the natural gas hydrates, oil and gas reservoir, or organic matter-rich anaerobic sediments, and then mixes with the surrounding water and finally forms buoyant plumes (Yin et al., 2008). A large amount of gas entering the sea water from the seafloor will inevitably result in a plume. The bubble-rich plumes have a strong scattering effect because of the large density and acoustic speed contrasts between the plumes

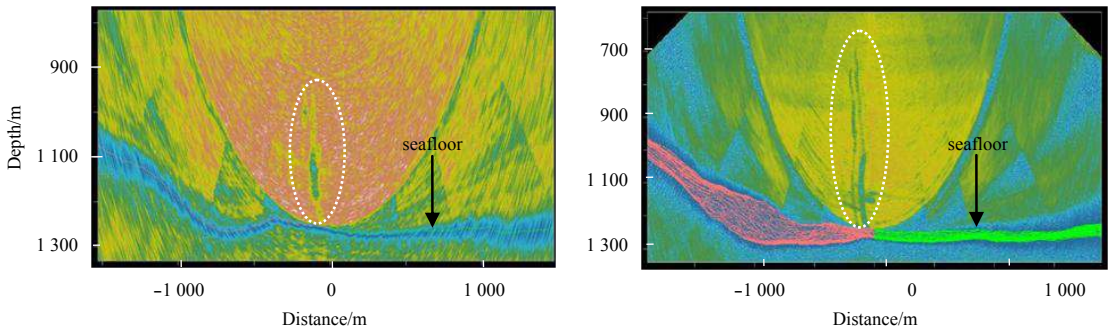

Fig. 5. Track cross-sections for Line 3.

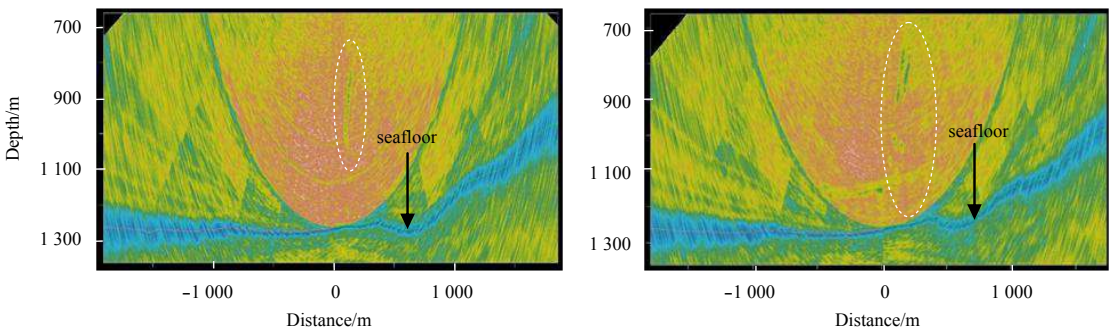

Fig. 6. Track cross-sections for Line 4.

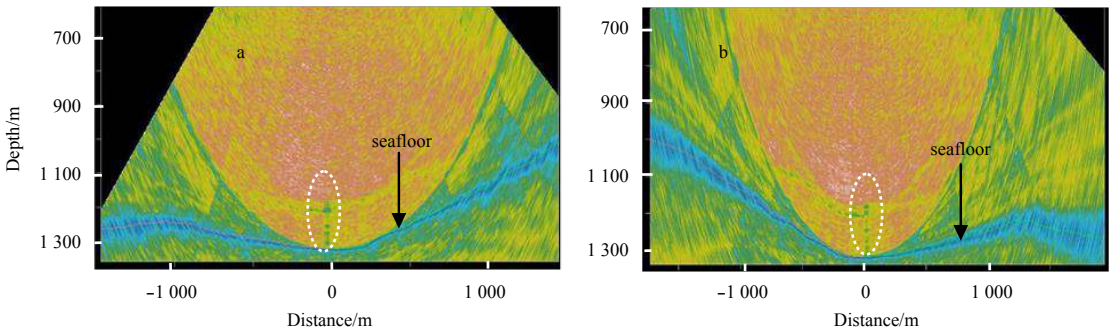

Fig. 7. Track cross-sections for Lines 5 (a) and 6 (b).

and ambient water (Kentaro et al., 2015). This allows gas seepages to be detected by an acoustic equipment.

There has been much integrated subsea floor geological exploration of the northern South China Sea, and this exploration has discovered many BSR and blanking zones as well as geochemical anomalies related to gas hydrates (Bi, 2010; He et al., 2006; Oung et al., 2006). All these discoveries illustrate the potential existence of natural gas hydrates in the research area. Yin et al. (2008) detected obvious methane density anomalies in the bottom water of the northern South China Sea. The anomalies resulted from methane seepage in the seafloor. The seepage may have originated from the decomposition of gas hydrates under the sediments. Bi (2010) analyzes the anomalous methane density in the bottom water of the southwest of Taiwan Island, and concludes that the anomalies are related to the seepage of methane generated from gas hydrate decomposition. The formation conditions for hydrates and the generation mechanism of the plumes indicate that there is not a one-to-one correspondence between hydrate and plume phenomena. However, seafloor sedimentary layers were often found in the development areas of plume, and plumes have been found in many sea areas where hydrates are found (Li et al., 2013, 2016). The results of our study indicate that there is a large amount of evidence for hydrate existence in the study area, and thus it can be inferred that the reason for the occurrence of the abnormal acoustic water column is most likely plume formation by gas leakage from natural gas hydrate. However, because of the lack of seismic data in the study area, it is difficult to further investigate the gas source of the plume. The abnormal acoustic water columns in the research area ascend for 200–500 m and then disappear. The authors believe the plume to be gas hydrate-coated methane bubbles. When the plume reaches a certain height from the seafloor, gas hydrate crusts become unstable and gradually dissolve as the surrounding pressure varies (Kentaro et al., 2015; Sauter et al., 2006). The anomalies then abruptly disappear. The ascending height of the plume may be related to the seepage volume of natural gas and the stability of hydrates. Some plumes in Line 4 appear to have no root, probably because the poor quality data from the line prevents the bottom of the plume from being detected. Another possible reason for some plumes having no apparent root is that the plumes were curved because of currents and only the top of the plumes was detected (Liu and Liu, 2017).

4.2.2 *Topographic analysis of the research area*

The seafloor topography of the research area is shown in Fig. 8. The depth is 1 000–1 420 m. The research area is located between two gorges on the continental slope of the South China Sea. The topography is complex. The terrain tilts from the central part to the east and to the west. The central part is shallow, but the eastern and western parts are deep. The depth of the eastern part is 1 300 m, and the seafloor is flat. The terrain in the central part is complex. Two sea ridges extend from north to south. One ridge has a height difference of 220 m and extends from northwest to south, with steep sides on both sides of the ridge. The other ridge extends from northeast to south. Its height difference is 50 m, and both sides of the ridge slope gently. The two ridges join the south to form one sea ridge. An elliptical-shaped knoll is located between the two sea ridges. The long axis of the seamount is 3 000 m, and the short axis is 2 000 m, and the height difference is 200 m. The western part of the knoll is closely connected to the sea ridge.

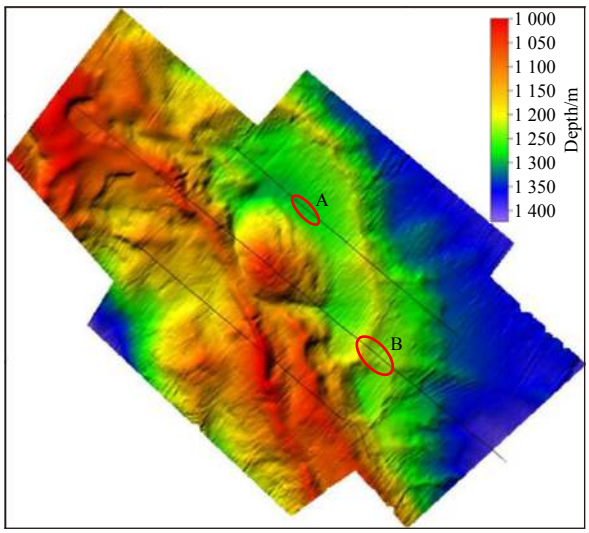

Fig. 8. Seafloor topography of the research area.

Obvious plumes are found in two positions in the research area (Fig. 8). Position A (Fig. 7) is located between two sea ridges. The water depth is 1 270–1 280 m. Position B (Figs 5 and 6) is located on a sea ridge, and the water depth is 1 210–1 230 m. The plume at Position B is the more obvious in the two of the water column images. This indicates a relatively high gas seepage speed at Position B.

Seafloor natural gas seepages can alter the seafloor terrain, and create unique micro-topography on the seafloor that includes such features as seabed pits, seabed mounds, and mud volcanoes (Liu, 2017; Shang et al., 2014; Sha et al., 2002; Chen et al., 2009). However, no obvious micro-topographic features were found in the plume areas in the present research. A possible reas-

on for this is that the speed and volume of gas seepage are low, and only result in small topographic alterations. These alterations are too small to be detected because of the resolution and accuracy of the shipborne multibeam system.

5 Conclusions

(1) Multibeam water column image anomalies were obtained for a new research area in the Taixinan Basin. The anomalies occur as single or multiple plumes, and ascend almost vertically from the seafloor to a height of 200–500 m.

(2) The plumes in the research area are possibly caused by methane seepage from the gas hydrate dissociation on the seafloor into the bottom water. The multibeam water column data reveal the possible existence of gas hydrates and provide a target for the future study of gas hydrate in this area.

(3) The successful detection of plumes in the Taixinan Basin using the multibeam sonar system has shown that the system can precisely locate in the position of plumes. Compared with the seismic detection technology, the multibeam sonar system has a fuller coverage, higher resolution, and higher efficiency. The multibeam sonar provides a systematic and reliable technology for the detection of subsea gas hydrate.

Acknowledgements

We thank the crew and scientific party of the R/V *Xiangyanghong No.18* for their kind support in the 2016 scientific expedition.

References

Bayrakci G, Scalabrin C, Dupré S, et al. 2014. Acoustic monitoring of gas emissions from the seafloor: Part II. A case study from the sea of Marmara. Marine Geophysical Research, 35(3): 211–229, doi: 10.1007/s11001-014-9227-7

Bi Haibo. 2010. Amount estimation and geochemical analysis of gas hydrate of Taixinan Basin (in Chinese) [dissertation]. Beijing, China: Graduate University of Chinese Academy of Sciences

Chen Shenhong, He Zhenhua, He Jiaxiong, et al. 2009. The characters of the mud volcanoes in the north-east marginal of the South China Sea and the relationship with the accumulation and migration of oil and gas. Natural Gas Geoscience (in Chinese), 20(6): 872–878

Chen S C, Hsu S K, Tsai C H, et al. 2010. Gas seepage, pockmarks and mud volcanoes in the near shore of SW Taiwan. Marine Geophysical Researches, 31(1–2): 133–147, doi: 10.1007/s11001-010-9097-6

Colbo K, Ross T, Brown C, et al. 2014. A review of oceanographic applications of water column data from multibeam echosounders. Estuaries, Coastal and Shelf Science, 145: 1–56, doi: 10.1016/j.ecss.2014.04.009

Du Deli. 1991. Characteristics of geologic structure and hydrocarbon potential of the southwest Taiwan Basin. Marine Geology & Quaternary Geology (in Chinese), 11(3): 21–33

Du Deli. 1994. Tectonic evolution and analysis of oil-gas accumulation in southwest Taiwan Basin. Marine Geology & Quaternary Geology (in Chinese), 14(3): 5–18

Elhegazy H. 2011. Gas plumes analysis using multibeam EM710 water column image in Saint John River. http://omg.unb.ca/omg/papers/Elhegazy_6922_Report.pdf [2011–10–11/2015–06–08]

He Jiaxiong, Xia Bin, Wang Zhixin, et al. 2006. Petroleum geologic characteristics and exploration base of Taixinan Bbasin in eastern area of continental shelf in north of the South China Sea. Natural Gas Geoscience (in Chinese), 17(3): 345–350

Kentaro Nakamura, Shinsuke kawagucc, Kazuya kitada, et al. 2015. Water column imaging with multibeam echo-sounding in the mid-Okinawa Trough: Implications for distribution of deep-sea hydrothermal vent sites and the cause of acoustic water column anomaly. Geochemical Journal, 49: 579–596, doi: 10.2343/geochemj.2.0387

Li Canping, Liu Xuewei, Zhao Luochen, et al. 2013. Progress on cold seeps and bubble plumes produced by gas hydrate. Progress in Geophysics (in Chinese), 28(2): 1048–1056

Li Canping, You Jiachun, Zhu Wenjuan. 2016. Identification of bubble plumes and analysis of its correlation with resource environment. Progress in Geophysics (in Chinese), 31(6): 2747–2755

Liu Zhibo. 2013. The least depth point detection of wreck using multibeam water column imaging (in Chinese)[dissertation]. Qingdao: Shandong University of Science and Technology

Liu Bin. 2017. Gas and gas hydrate distribution around seafloor mound in the Dongsha area, north slope of the South China Sea. Haiyang Xuebao (in Chinese), 39(3): 68–75

Liu Bin, Liu Shengxuan. 2017. Gas bubble plumes observed at north slope of South China Sea from multibeam water column data. Haiyang Xuebao (in Chinese), 39(9): 83–89

Luan Xiwu, Zhao Kebin, Sun Dongsheng, et al. 2008. Geophysical methods for marine gas hydrates exploration. Progress in Geophysics (in Chinese), 23(1): 210–219

Ma Yong. 2016. Sediment waves characteristics and their formation mechanism, the southwest Taiwan Basin, South China Sea (in Chinese) [dissertation]. Nanjing: Nanjing University

Melvin G D, Cochrane N A. 2015. Multibeam acoustic detection of fish and water column targets at high-flow sites. Estuaries and Coasts, 38(S1): S227–S240, doi: 10.1007/s12237-014-9828-z

Nakamura K, Kawagucc S, Kitada K, et al. 2015. Water column imaging with multibeam echo-sounding in the mid-Okinawa Trough: implications for distribution of deep-sea hydrothermal vent sites and the cause of acoustic water column anomaly. Geochemical Journal, 49(6): 579–596, doi: 10.2343/geochemj.2.0387

Oung J N, Lee C Y, Lee C S, et al. 2006. Geochemical study on hydrocarbon gases in seafloor sediments, southwestern offshore Taiwan-Implications in the potential occurrence of gas hydrates. Terrestrial, Atmospheric and Oceanic Sciences, 17(4): 921–931, doi: 10.3319/TAO.2006.17.4.921(GH)

Sauter E J, Muyakshin S I, Charlou J L, et al. 2006. Methane discharge from a deep-sea submarine mud volcano into the upper water column by gas hydrate-coated methane bubbles. Earth and Planetary Science Letters, 243(3–4): 354–365, doi: 10.1016/j.epsl.2006.01.041

Sha Zhibin, Yang Muzhuang, Liang Jin, et al. 2002. The characteristics of the abnormal physiognomys of seabed related to gas hydrate in North Slope, South China Sea. Geological research on the South China Sea (in Chinese), (1): 29–34

Shang Jiujing, Wu Lushan, Liang Jinqiang, et al. 2014. The microtopographic features and gas seep model on the slope in the northeastern South China Sea. Marine Geology & Quaternary Geology (in Chinese), 34(1): 129–136

Xu Huaning, Xing Tao, Wang Jiasheng, et al. 2012. Detecting seepage hydrate reservoir using multi-channel seismic reflecting data in Shenhu area. Earth Science-Journal of China University of Geosciences (in Chinese), 37(S1): 195–202

Yang Fanlin, Han Litao, Wang Ruifu, et al. 2013. Progress in object detection in middle and bottom-water based on multibeam water column image. Journal of Shandong University of Science and Technology: Natural Science (in Chinese), 32(6): 75–83

Yin Xijie, Zhou Huaiyang, Yang Qunhui, et al. 2008. The evidence for the existence of methane seepages in the northern South China Sea: abnormal high methane concentration in bottom waters. Haiyang Xuebao (in Chinese), 30(6): 69–75

Zhang Guangxue, Liang Jinqiang, Lu Jing'an, et al. 2014. Characteristics of natural gas hydrate reservoirs on the northeastern slope of the South China Sea. Natural Gas Industry (in Chinese), 34(11): 1–10

Zheng Shuangqiang, Liu Hongxia, Yang Fanlin, et al. 2016. Design and implementation of multibeam sonar water column image analysis toolkit. Hydrographic Surveying and Charting (in Chinese), 36(6): 46–49